What You See is (Usually) What You Get: Multimodal Prototype Networks that Abstain from Expensive Modalities

Muchang Bahng* Duke University

muchang.bahng@duke.edu

Jon Donnelly Duke University

jon.donnelly@duke.edu

Charlie Berens* Duke University

cjb131@duke.edu

Chaofan Chen University of Maine

chaofan.chen@maine.edu

Eric Chen Duke University

eric.y.chen@duke.edu

Cynthia Rudin Duke University

cynthia@cs.duke.edu

Abstract

Species detection is important for monitoring the health of ecosystems and identifying invasive species, serving a crucial role in guiding conservation efforts. Multimodal neural networks have seen increasing use for identifying species to help automate this task, but they have two major drawbacks. First, their black-box nature prevents the interpretability of their decision making process. Second, collecting genetic data is often expensive and requires invasive procedures, often necessitating researchers to capture or kill the target specimen. We address both of these problems by extending prototype networks (ProtoPNets), which are a popular and interpretable alternative to traditional neural networks, to the multimodal, cost-aware setting. We ensemble prototypes from each modality, using an associated weight to determine how much a given prediction relies on each modality. We further introduce methods to identify cases for which we do not need the expensive genetic information to make confident predictions. We demonstrate that our approach can intelligently allocate expensive genetic data for fine-grained distinctions while using abundant image data for clearer visual classifications and achieving comparable accuracy to models that consistently use both modalities.

1. Introduction

In biological domains such as ecology and healthcare, machine learning tools have been used to help professionals make more informed decisions. These high-stakes problems often use multiple streams of data. For example, doctors may consider a patient's self-described symptoms, blood test results, x-rays, blood pressure, and stethoscope findings before making a diagnosis. Similarly, ecologists

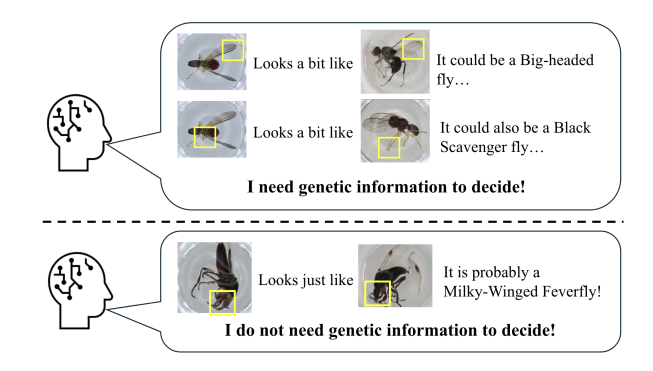


Figure 1. In practice, some samples are easier to classify than others – if visual information is sufficient to classify a sample, we need not measure genetic information. Our models intelligently decide when they can abstain from measuring genetic information while maintaining accuracy and follow a transparent reasoning process.

may not be able to classify an organism solely based on visual data, needing some form of audio or genetic data to differentiate similar-looking species. This suggests a more general challenge: how to use different data modalities effectively.

Multimodal neural networks have been effective in analyzing multiple modalities of data, achieving state-of-theart performance in a variety of tasks [11, 22]. However, they have two major drawbacks. First, they are fundamentally black-box in nature, which prevents professionals from interpreting the decision-making process of these models. Second, not all data are equal. In practice, data type A (e.g., images of organisms) may be much more accessible than data type B (e.g., genetic sequences), although B may be more informative. Therefore, during inference, we may prefer our models to use only data A if possible and avoid B unless it is absolutely necessary. Doing so can greatly

^{*}Equal contribution.

reduce the cost of expensive or invasive procedures with a minimal (or no) decrease in accuracy. Figure 1 provides a high level overview of the reasoning process we develop.

In computer vision, prototype networks (ProtoPNets) are an emerging approach to designing interpretable neural networks, offering the predictive power of neural networks while providing an inherently interpretable reasoning process [3]. ProtoPNet and its variants [7, 8, 15, 16, 20, 23, 24, 28–30, 32] utilize a case-based reasoning process in which a set of learned prototypical examples of each class is compared to a given input to form predictions. We introduce two novel approaches to combine image and genetic modalities, while abstaining from measuring genetic data when possible:

Conformal Abstention Learning (CAL) CAL is a general technique that can be used beyond image and genetic data. The steps for CAL are as follows: (1) Determine which modality is most expensive. Here, genetic data are most expensive. (2) Apply conformal prediction to determine the maximum reasonable change in our predicted logits due to measuring the expensive modality. (3) Determine if the maximum reasonable change would be sufficient to alter our overall prediction. If not, we do not need to measure the genetic information.

Abstention Learning ProtoTree. (ALP) This is a specialized multimodal extension of ProtoTree [20] in which each internal node may consider either a genetic or an image prototype comparison. We leverage ProtoTree's unique tree structure to regularize towards one modality when forming predictions by encouraging entire paths from root to leaf to use only image information.

We apply CAL and ALP to the BIOSCAN-1M insect classification dataset, which contains paired image and genetic information for 516 insect species. At inference time, our models consider whether the more expensive modality (genetic information) is necessary to make a prediction; when it is not, they reason solely based on the less expensive modality (in this case, images). We demonstrate that, by identifying cases that are easy to classify with image information alone, we can achieve comparable accuracy to full multimodal models with just a fraction of the genetic information needed overall, all while providing an interpretable reasoning process.

2. Related Works

Image-Genetic Species Classification. Deep neural networks have been successfully deployed to classify species based on image data [17] or genetic data [2, 9] across a variety of settings. Recently, the research community has expanded on these methods by leveraging both modalities for species classification through a shared embedding space [11], by ensembling distinct representations of image and genetic data [18, 19], and by combining both modalities

for better out-of-distribution detection [12]. However, these methods all follow an opaque reasoning process, raising concerns about their reliability in deployment.

Case-Based Neural Networks. In an orthogonal line of work, researchers have developed interpretable, case-based deep neural networks for classification tasks [3, 14]. Given an input, these models first extract features using a neural network backbone, then make comparisons to a set of learned prototypes using these extracted features. This comparison yields a similarity score for each prototype, and these scores are combined to form a class prediction, yielding an explanation of the form "this looks like that". Since the introduction of the first of these models - called ProtoPNet [3] - a wide variety of improvements and extensions to this framework have been developed [7, 8, 15, 16, 20, 23, 24, 28–30, 32]. The majority of these models form their classifications using a linear combination of the prototype similarity scores [7, 8, 15, 16, 28– 30, 32]. In contrast, ProtoTree [20] learns a decision tree in which each internal node performs a prototype comparison, and each leaf specifies a vector of class logits.

While these models have primarily been used for image classification, recent extensions have turned to consider additional data modalities. Notably, Waggoner et al. [28] applied this case based reasoning approach to environmental DNA classification. Wang et al. [31] extended ProtoPNet to consider both image and text data, while Song et al. [25] considered text, image, and acoustic modalities. Yang et al. [34] combines four medical data modalities, including images and a table of gene expression levels. However, no case-based method exists to consider image and raw basepair genetic sequences (rather than tabular expression levels); moreover, existing multimodal extensions of ProtoPNet assume that every data modality is available for every sample. We leverage ideas from conformal prediction and prediction abstention to address this gap.

Abstention and Conformal Predictions In this work, we draw inspiration from the problem of classification with the option to abstain from making a prediction [1, 4, 5], in which classifiers are encouraged to refrain from making predictions in cases where they are likely to be incorrect. In the same spirit, our aim is to measure genetic information about a sample only when an image classifier abstains from making a prediction.

We use conformal prediction [13, 21, 27] to identify cases in which an image classifier should abstain. Conformal prediction uses a held out calibration set to estimate quantiles for the error of an arbitrary model with respect to a target, providing statistically rigorous prediction intervals. We frame the task of identifying cases where an image classifier should abstain as a multi-output regression task

(explained in Section 3) and leverage specialized conformal prediction methods for this setting [6].

3. Methodology

Let $\mathbf{x} \in \mathbb{R}^{C \times H \times W}$ denote an input image or sequence of height H and width W with C channels, and let $\mathbf{v} \in$ $\{0,\ldots,K-1\}$ denote class labels. For simplicity of notation, we generally define our models and loss terms with respect to a single sample (x, y) and omit subscripts that distinguish between different samples in a dataset. Following the standard interface of ProtoPNext [33], a ProtoPNet consists of an embedding layer $f: \mathbb{R}^{C \times H \times W} \rightarrow$ $\mathbb{R}^{D\times H'\times W'}$, which extracts a $H'\times W'$ map of D dimensional feature vectors; a prototype layer $g:=g_2\circ g_1$, where $g_1:\mathbb{R}^{D\times H'\times W'}\to\mathbb{R}^{P\times H''\times W''}$ computes the similarity of each of the P learned prototypes to the input at each of $H'' \times W''$ locations and $g_2 : \mathbb{R}^{P \times H'' \times W''} \to \mathbb{R}^P$ computes the maximum value over these spatial locations; and a class prediction head $h: \mathbb{R}^P \to \mathbb{R}^K$ that uses these prototype similarities to compute an output logit for each class. For conciseness of notation, we define z := f(x) to be the latent representation of input x, $s := g \circ f(x)$ to be the maximum similarity between each prototype and the input at any spatial location, and $\hat{\mathbf{y}} := h \circ g \circ f(\mathbf{x})$ to be a vector of class logits. Broadly, these models minimize a loss function of the form

$$\ell(f, g, h, \mathbf{x}, \mathbf{y}) = CE(h \circ g \circ f(\mathbf{x}), \mathbf{y}) + \ell'(f, g, h, \mathbf{x}, \mathbf{y})$$

where CE denotes the cross-entropy loss, and ℓ' is a combination of regularization penalties and interpretability metrics. Furthermore, in almost all ProtoPNet variants, a prototype projection step is performed during and at the end of training to associate each learned prototype with a specific pixel space visualization.

We consider the setting where both image and genetic data may be available for a given sample, which we denote by $\mathbf{x}^{(I)} \in \mathbb{R}^{3 \times 224 \times 224}$ and $\mathbf{x}^{(G)} \in \mathbb{R}^{4 \times 1 \times 720}$ respectively. Here, our genetic data is comprised of variable-length strings denoting nucleotides (A,C,T,G) that are right-padded, and then one-hot encoded into a tensor in $\mathbb{R}^{4 \times 1 \times 720}$. In each of our approaches, we consider two ProtoPNets, $F^{(I)} := h^{(I)} \circ g^{(I)} \circ f^{(I)}$ and $F^{(G)} := h^{(G)} \circ g^{(G)} \circ f^{(G)}$, to separately process image and genetic data, respectively. Figure 2 provides an overview of our two approaches in combining the two modalities.

3.1. Conformal Abstention Learning (CAL)

We first consider ensembling $F^{(I)}$ and $F^{(G)}$ through a simple class-wise weighted average of the logits from each model. For class j, the final output logit \hat{y}_j of the multimodal model is a weighted average of the corresponding

image and genetic logits:

$$\hat{y}_j = \sigma(m_j) F_j^{(I)}(\mathbf{x}^{(I)}) + (1 - \sigma(m_j)) F_j^{(G)}(\mathbf{x}^{(G)}),$$

where $m_j \in \mathbb{R}$ is a learnable parameter that determines how much the final output logit depends on its corresponding image and genetic logits.

We now introduce the application of conformal prediction to this task, then introduce loss terms that aim to make the model weigh one modality more highly than the other.

3.1.1. Conformal Prediction

The construction of our multimodal model separates out the contribution of each genetic logit $F_j^{(G)}(\mathbf{x}^{(G)})$ from that of each image logit $F_j^{(I)}(\mathbf{x}^{(I)})$. As such, if we can bound the values that $(1-\sigma(m_j))F_j^{(G)}(\mathbf{x}^{(G)})$ could take, we can bound how much the overall value of each logit \hat{y}_j might change relative to $F_j^{(I)}(\mathbf{x}^{(I)})$.

We leverage split conformal prediction to form these bounds. Given a prediction, split conformal prediction provides a prediction set for its true value with some user-specified confidence value $1-\alpha$. It does so by calibrating the model's residuals on a held-out calibration set to estimate the distribution of prediction errors.

To predict each *genetic* logit, we introduce an additional fully connected layer $\hat{h}: \mathbb{R}^P \to \mathbb{R}^K$ to the *image* model to predict the *genetic* logits $\hat{\mathbf{y}}^{(G)}$. It is initialized with the same weights as $h^{(I)}$, and is trained to minimize the mean squared error between each prediction and $\hat{\mathbf{y}}^{(G)}$.

Let δ_j denote the margin of error of the prediction set for logit \hat{y}_j , and let k be the class predicted by $F^{(I)}$ for an input $\mathbf{x}^{(I)}$. Then, with probability at least $1 - \alpha$, the genetic data could not yield a more different set of predicted logits than

$$\tilde{y}_j = \begin{cases} \sigma(m_j) \hat{y}_j^{(I)} + (1 - \sigma(m_j)) (\hat{y}_j^{(G)} - \delta_j) & \text{if } j = k \\ \sigma(m_j) \hat{y}_j^{(I)} + (1 - \sigma(m_j)) (\hat{y}_j^{(G)} + \delta_j) & \text{otherwise.} \end{cases}$$

That is, the logit for the predicted class k based on the image data \hat{y}_k is unlikely to decrease past \tilde{y}_k , and every other logit \hat{y}_j is unlikely to increase past \tilde{y}_j . If $\arg\max\tilde{\mathbf{y}}=k$, then with $(1-\alpha)$ confidence, we know that introducing genetic information cannot change the prediction from that of the image model. Figure 3 visualizes this logic.

It is worth noting that we compute a distinct marginal conformal interval for each genetic logit; as such, for full statistical rigor, a correction for multiple hypothesis testing should be applied. In practice, we observe that this is not necessary to achieve nominal coverage rates, as demonstrated in Section 4.

Now that we know how to evaluate models for abstention, we turn to how to train models to abstain more often.

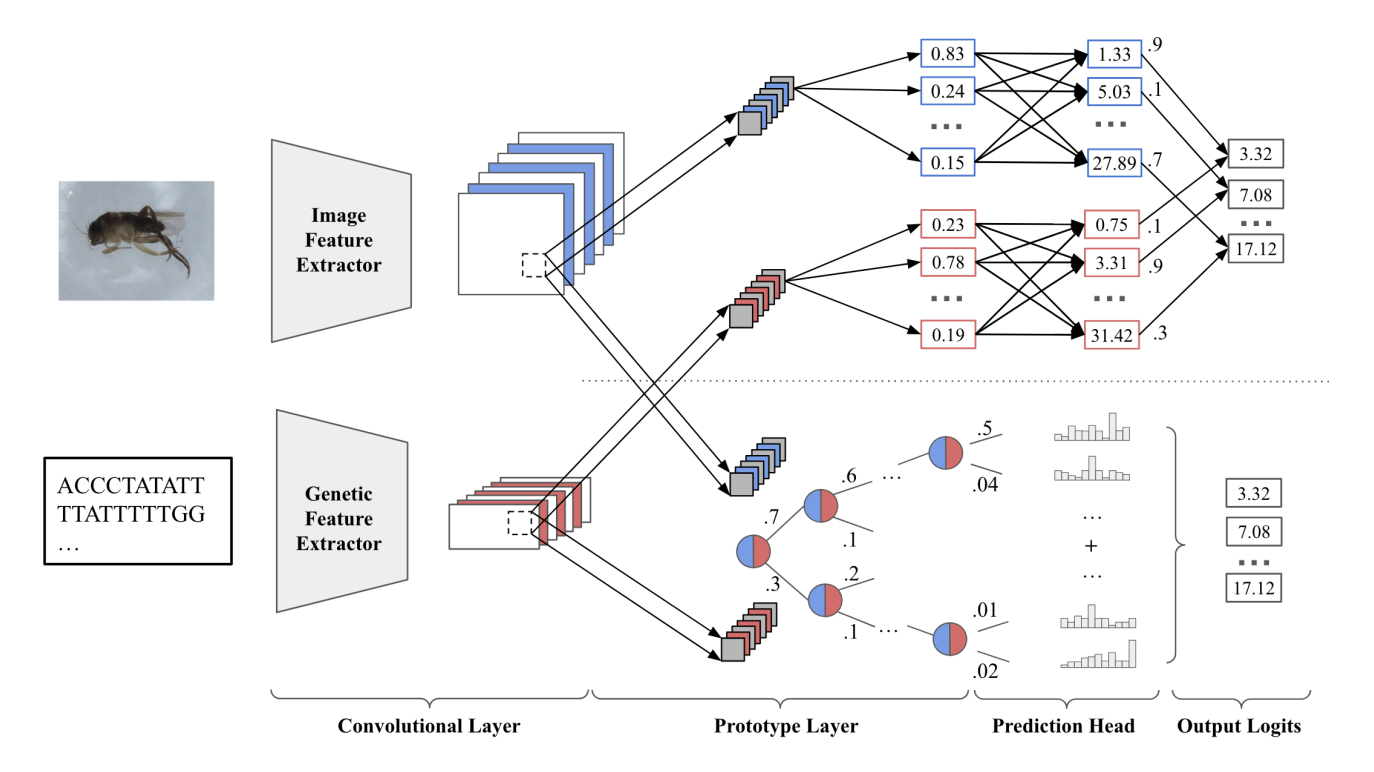


Figure 2. Our multimodal extensions applied to a vanilla ProtoPNet (top) and a ProtoTree (bottom). Both architectures use the same pair of convolutional feature extractors on image and genetic data. In the ProtoPNet, we take a weighted average of the logits using CAL. In the ProtoTree, we consider either a genetic or an image prototype at each node in the tree and traverse the tree based on the prototype's similarity to the input. Some paths from the root to the leaf do not require consideration of any genetic prototypes, while others do.

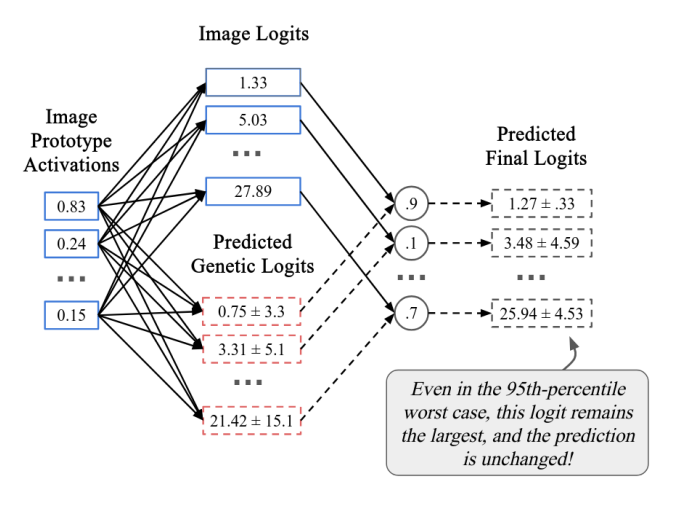


Figure 3. The prediction head of a multimodal ProtoPNet employing conformal prediction to produce prediction sets for CAL. The image prediction head includes an additional fully connected layer to predict the genetic logits, and conformal prediction is employed to create prediction sets around them.

3.1.2. Loss Terms

The conformal prediction method of Subsection 3.1.1 can be applied to any pair of models, but may not always yield tight intervals. Here, we introduce two loss terms aimed at helping to achieve tighter intervals.

To encourage the model to abstain from measuring genetic information when possible, we introduce a *margin loss* to increase the distance between the worst-case logits and the decision boundary. Let $d_j := \tilde{y}_k - \tilde{y}_j$. If $\min_{j \neq k} d_j > 0$, then \tilde{y}_k is still the maximum logit, and the classification is unlikely to be changed by genetic information.

Directly maximizing the margin $\min_{j\neq k} d_j$ passes gradients through a single logit, leading to slow convergence. We instead maximize a soft minimum of d_j , defining margin loss as:

$$\ell_{ ext{margin}} := \log \left(\sum_{j=0, j
eq k}^{K-1} e^{-d_j}
ight).$$

Additionally, we can reduce the maximum possible contribution of any given genetic logit by increasing the value of each $\sigma(m_i)$, thereby decreasing the weight $1 - \sigma(m_i)$ as-

signed to the genetic logit:

$$\ell_{\text{modality}} := -\sum_{j=0}^{K-1} \sigma(m_j).$$

To train the genetic logit predictor \hat{h} , we include a loss term defined as the mean squared error between the true genetic logits and their predicted values.

$$\ell_{\text{predictor}} := \frac{1}{K} \sum_{j=0}^{K-1} \left(\hat{y}_j^{(G)} - \hat{h}_j(g^{(I)}(f^{(I)}(\mathbf{x}_i^{(I)})) \right)^2$$

3.1.3. Optimization

To train the multimodal ProtoPNet, we first initialize the model with a ProtoPNet trained for each modality, and freeze all but the modality weights and the fully-connected layers. We then minimize the overall loss:

$$\ell_{total} := \ell_{CE} + \lambda_1 \ell_{\text{modality}} + \lambda_2 \ell_{\text{margin}} + \lambda_3 \ell_{\text{predictor}}$$

The cross-entropy loss ℓ_{CE} operates on the image logits alone when image data is deemed sufficient at a pre-set confidence value, otherwise it operates on the final multimodal logits.

3.2. Abstention Learning ProtoTree (ALP)

Here, we introduce a specialized cost-aware multimodal extension of ProtoTree [20]. We first introduce the original ProtoTree. In ProtoTree, the class prediction head h^{tree} is structured as a full binary decision tree consisting of a set of P internal nodes $\mathcal N$ and a set of leaf nodes $\mathcal L$. Each internal node $n \in \mathcal N$ is associated with two child nodes, denoted $n_{\text{left}} \in \mathcal N \cup \mathcal L$ and $n_{\text{right}} \in \mathcal N \cup \mathcal L$, which are traversed in a soft manner — that is, the left and right sub-tree of each node are both involved in forming a prediction — based on s_n for a given input. Each leaf node $l \in \mathcal L$ contains an associated logit vector, which we denote $\hat{\mathbf y}_l$. The full prediction head h^{tree} for a ProtoTree is thus defined recursively as:

$$h^{\text{tree}}(\mathbf{s}) := r(n_{\text{root}}, \mathbf{s}), \text{ where }$$

$$r(n,\mathbf{s}) := \begin{cases} (1-s_n)r(n_{\text{left}},\mathbf{s}) + s_n r(n_{\text{right}},\mathbf{s}) & \text{if } n \in \mathcal{N} \\ \hat{\mathbf{y}}_l & \text{if } n \in \mathcal{L} \end{cases},$$

where $n_{\rm root}$ denotes the root node and s is the vector of prototype similarity scores. This formula signifies that the output is a weighted average of contributions from the leaves, where each leaf calculation is based on how similar the input is to each prototype at each node along the path to the leaf. In a unimodal ProtoTree, we compute either $h^{\rm tree}(\mathbf{s}^{(I)})$ or $h^{\rm tree}(\mathbf{s}^{(G)})$, depending on the modality.

As in the original paper, we train using the soft traversal function $h^{\rm tree}$ but employ hard decision routing at test time

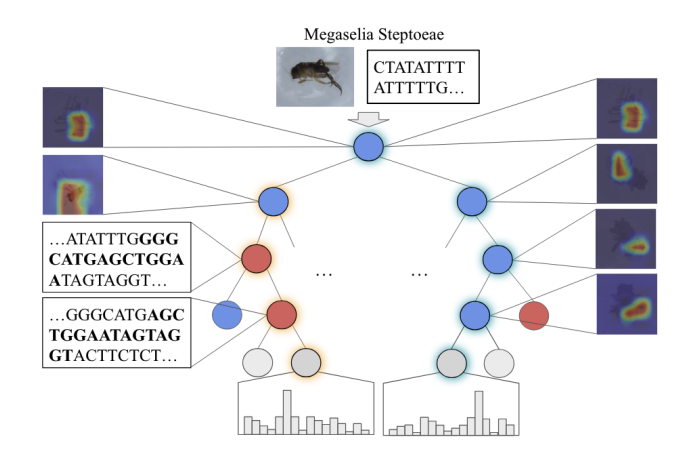


Figure 4. Example reasoning from a trained ALP. Given an input consisting of image and genetic data, we present two possible paths (indicated by highlighted nodes) in which a multimodal ProtoTree may route it to a leaf. In the left path, the first two nodes consider image prototypes and the last two consider genetic prototypes. If the image is routed down this path, we must measure genetic information. The right path, on the other hand, only considers image prototypes. We do not need to measure genetic information for images routed down this path.

by greedily traversing the tree, i.e., go right at internal node n if $s_n>0.5$ and left otherwise. We call this traversal function $h^{\rm tree,hard}$.

In ALP, each node n considers the prototype similarity vector from each modality ($\mathbf{s}^{(I)}$ and $\mathbf{s}^{(G)}$), plus a *modality* weight $m_n \in \mathbb{R}$ that determines how much each modality should contribute to the left/right routing. We define the multimodal similarity (for the multimodal tree) as a combination of the similarities to image and genetic prototypes:

$$s_n^{(I+G)} := \sigma(m_n)s_n^{(G)} + (1 - \sigma(m_n))s_n^{(I)},$$

where σ is the sigmoid function. Given $\mathbf{s}^{(I+G)}$, the prediction of our multimodal ProtoTree is then computed as $h^{\text{tree}}(\mathbf{s}^{(I+G)})$, with h^{tree} defined as before and used in training, and $h^{\text{tree},\text{hard}}$ defined as before, used at test time.

3.2.1. Threshold Based Modality Assignment

When one modality is more expensive to collect than the other, users may wish to guide which modality the ProtoTree emphasizes. We leverage a specialized initialization strategy to encourage our ALP model to only use image information when it is sufficient for a strong classification.

Given a trained image-only ProtoTree $F^{(I)}$ and a leaf node $l \in \mathcal{L}$, let \mathcal{D}_l be the subset of our dataset that is routed to l during a hard traversal of the image-only ProtoTree, and let $\mathcal{N}_l \subset \mathcal{N}$ be the set of all internal nodes in the path from n_{root} to l. For each sample $(\mathbf{x}^{(I)}, \mathbf{y}^{(I)}) \in \mathcal{D}_l$, denote

$$\mathrm{acc}_l = \mathbb{P}\left(F^{(I)}(\mathbf{x}^{(I)}) = \mathbf{y}^{(I)} \mid (\mathbf{x}^{(I)}, \mathbf{y}^{(I)}) \in \mathcal{D}_l\right)$$

That is, acc_l denotes the accuracy of a leaf in classifying samples that reach l during a hard traversal. We aim to keep all image nodes that lead to accurate classification and replace the ineffective ones with genetic nodes by defining a threshold $t \in [0, 1]$, and initializing the set of internal nodes

$$\mathcal{N}_t = \{ n \in \mathcal{N} \mid n \in \mathcal{N}_l, \mathrm{acc}_l > t \}$$

that contribute to these high-accuracy image decisions to have image-only modalities. That is, we set $m_n = \tau$ if $n \in \mathcal{N}_t$, and $m_n = \tau$ otherwise for some positive value τ . By doing so, we preserve the performance of the unimodal image ProtoTree for $n \in \mathcal{N}_t$, whilst maximally exploiting the genetic prototypes for all subsequent splits. A natural value for the threshold t is the accuracy of the genetic unimodal ProtoTree, which indicates that we only want to keep nodes that lead to predictions that are at least as confident as the genetic ProtoTree. If we set τ to a very large value, then it is equivalent to deleting the subtrees whose leaves all have low accuracy; those subtrees will be replaced with genetic subtrees.

3.2.2. Deterministic Modality Routing

During training of the multimodal tree, which is trained from both image and genetic data, we do not constrain m_n , but we apply a regularization term encouraging the modality weights of each node to polarize towards $+\infty$ or $-\infty$ so that only one modality will be used. We apply an entropy-based polarization term to the probability space as:

$$\ell_{routing} = \frac{1}{P} \sum_{n=0}^{P-1} \left(\sigma(m_n) \log(\sigma(m_n)) + (1 - \sigma(m_n)) \log(1 - \sigma(m_n)) \right).$$

To maintain simple interpretations, we clip the modality weights m_n to $\pm \infty$ at the end of training to ensure that at each split, an internal node will either solely observe an image prototype or a genetic prototype.

3.2.3. Optimization Objective

To train the multimodal ProtoTree, we first trained two models: an image-only ProtoTree and a genetic ProtoTree. We initialize the multimodal ProtoTree using the convolutional weights and prototypes from both networks. We also use the image-only ProtoTree to initialize our modality weights using threshold based modality assignment. For paths that end with an image prototype, we initialize the leaf in that path using the corresponding logit vector from the image ProtoTree; otherwise, we use the logit from the genetic ProtoTree. We then freeze the image-only ProtoTree weights and train the genetic part of the multimodal model to minimize the overall loss:

$$\ell_{total} = \ell_{CE} + \lambda_1 \ell_{cluster} + \lambda_2 \ell_{ortho} + \lambda_3 \ell_{var} + \lambda_4 \ell_{wd} + \lambda_5 \ell_{routing}$$

where $\ell_{cluster}$ is the cluster loss from [20], ℓ_{ortho} is the orthogonality loss from [32], ℓ_{wd} is weight decay, and ℓ_{var} is a variability loss that aims to encourage diversity among prototype activations, defined as

$$\ell_{var} = -\frac{1}{H''W''} \sum_{h=1}^{H''} \sum_{w=1}^{W''} \mathbb{V}[(g_1 \circ f(\mathbf{x}))_{h,w}],$$

where \mathbb{V} denotes the finite sample variance taken over the P entries in $(g_1 \circ f(\mathbf{x}))_{h,w}$. We perform prototype projection at the end of training, as defined in [3].

4. Experiments

We evaluated the performance of our multimodal models for species classification using the BIOSCAN-1M insect classification dataset [10]. Though the dataset contains more than 1 million samples, only about 84,000 are labeled with a species. We employed a 60/20/20 train/validation/test split. For training our CAL model, the validation set was also used as the calibration set for our conformal intervals. The species distribution is extremely unbalanced and heavy-tailed, so we proportionally oversampled minority classes during training, and evaluated our results primarily on balanced accuracy. To evaluate our ability to prioritize using only image data, we introduce a new metric: success rate. Success rate is defined as the percentage of samples classified using exclusively image data, where a higher success rate indicates more samples were classified without genetic data. See the supplement for more details regarding our experimental setup.

We used a ResNet-50 backbone pretrained on iNaturalist for our image modality, and a shallow CNN (described in the supplement) backbone for our genetic modality. Our CAL and ALP models were initialized with trained image and genetic ProtoPNet and ProtoTree models, respectively. A more detailed set of hyperparameter and architecture settings is provided in the supplement.

We optimized each ProtoPNet, including baseline models, using Bayesian hyperparameter optimization for 36 GPU hours, allowing runs that started before the time limit to train to completion. We evaluate a multimodal ProtoPNet as an instance of CAL, and a multimodal ProtoTree as an instance of ALP.

4.1. Quantitiative Results

Our experiments show that CAL and ALP can achieve high balanced accuracy while querying less genetic data. As shown in Figure 5, both our multimodal ProtoPNet and ProtoTree can achieve competitive accuracies with their genetic counterparts while using substantially less genetic data. For the multimodal ProtoPNet at a confidence value $\alpha = .05$, we see a drop in balanced accuracy of only 0.84% compared to a genetic ProtoPNet, while gaining a 40.26%

Success Rate and Accuracy at Different Thresholds

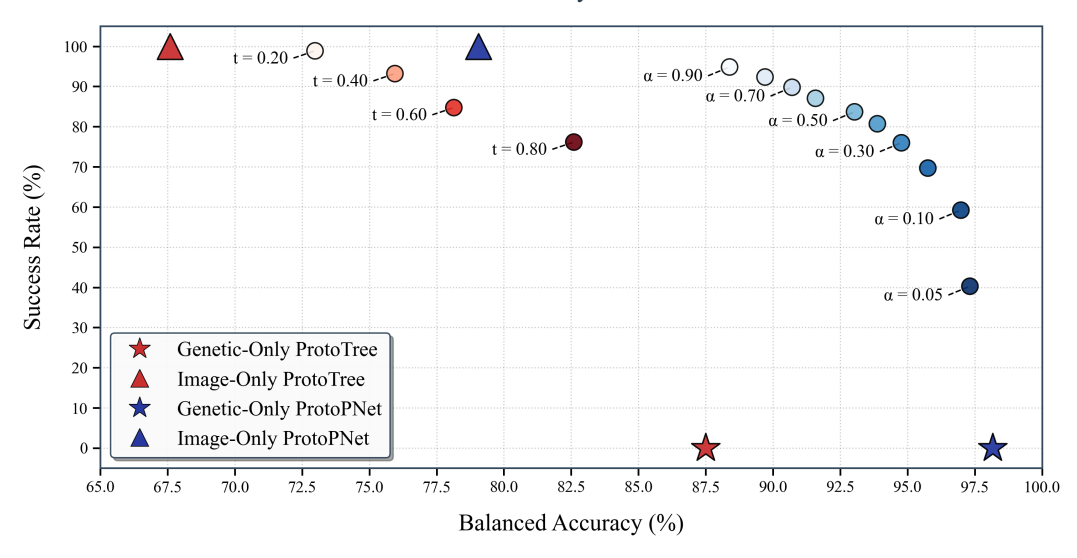


Figure 5. Balanced accuracy vs success rate for ALP and CAL models. Red is for ProtoTree and blue is for ProtoPNet. We see that there is a very small loss in accuracy for a very large boost in success rate at small values of α for CAL; with $\alpha=0.1$, there is a 0.5% decrease in accuracy from the most accurate ProtoPNet, in exchange for 59.20% success rate. In ALP, we see that there is a larger trade-off, with a 5% decrease in accuracy for 76.15% success rate, but that ALP is effective in obtaining high success rates.

	Image	Genetic	
ResNet-50	78.32 (100%)	-	
Genetic CNN	-	98.64 (0%)	
BioCLIP [26]	50.39 (100%)	-	
CLIBD [11]	51.39 (100%)	95.79 (0%)	
ProtoPNet [3]	79.06 (100%)	98.16 (0%)	
ProtoTree [20]	67.59 (100%)	87.50 (0%)	
Deformable [7]	78.71 (100%)	99.24 (0%)	
Support Trivial [29]	57.93 (100%)	88.57 (0%)	
CAL (α=0.00)	97.57 (0%)		
CAL (α =0.05)	97.32 (40.26%)		
ALP (t=0.8)	82.60 (76.15%)		
ALP (t=0.6)	78.14 (84.73%)		

Table 1. Accuracy comparison to prior work for species classification on BIOSCAN-1M Dataset. We report the balanced accuracy of each model on the test split, which contains 8,200 samples. The success rate of each model is reported in parentheses. The highest accuracy is in bold. While a genetic Deformable ProtoPNet achieves the highest accuracy, CAL achieves only 1.9% less accuracy while finding a success rate of 40.26%.

success rate, meaning we are able to classify 40.26% of the samples using only image information. In other words, this means that in 40.26% of cases, we would *not* have to collect expensive genetic data to make a classification. We see a moderate loss in accuracy (4.9%) between multimodal ProtoTree and genetic ProtoTree in exchange for a substantial 76.15% improvement in success rate with ALP.

	Balanced Accuracy	Success %
Mar. + Mod. Loss	97.32	40.26%
Mar. Loss	96.65	37.65%
Mod. Loss	94.14	61.61%
Neither Loss	97.13	10.39%

Table 2. Ablation on CAL for margin and modality loss. Metrics are reported for the best-performing CAL models with and without each loss. Metrics are evaluated at a confidence value of $\alpha=0.05.$ Mar. is margin loss, and Mod. is modality loss. Including both loss terms yields the best accuracy, with the second best success rate.

	Balanced Accuracy	Success %
Var. + Rout. Loss	82.60	76.15%
Var. Loss	81.75	76.15%
Rout. Loss	78.17	74.39%
Neither Loss	77.84	74.14%

Table 3. Ablation on ALP for variability and routing loss. Metrics are reported for the best-performing ALP model with threshold t=0.8, with and without each loss. Var is variability loss, and Rout is routing loss. Including both loss terms yields the best accuracy and the best success rate.

Our models produce comparable accuracy to baseline genetic only models. As seen in Table 1, both our multimodal ProtoPNet and ProtoTree models perform similarly to existing genetic models and consistently outperform existing image-based species classification models. We see

Error Rate at each Confidence Level

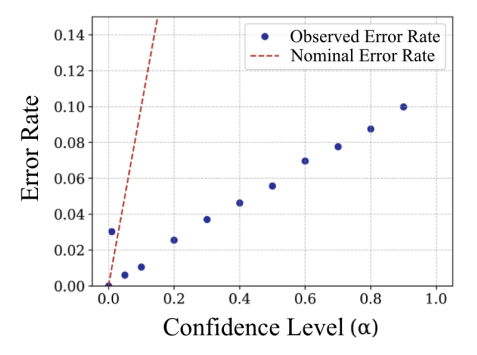


Figure 6. Error rate at each confidence level for CAL models. Here, we see that the error rate is often far below the target confidence level, meaning CAL rarely incorrectly abstains from gathering genetic information. This kind of error happens far below the nominal rate.

that CAL can achieve 97.57% balanced accuracy, competitive with genetic-only black-box models like a Genetic CNN at 98.64% and other interpretable models like vanilla ProtoPNet at 98.16%, while being slightly worse than Deformable ProPNet at 99.24%. For ALP, we see that it only gets a balanced accuracy of 82.60%; this mirrors the relatively low balanced accuracy of both image and genetic ProtoTree compared to other models. While we note that ALP does perform worse than the pure genetic models, this comes with a massive boost in success rate.

Our ablation experiments indicate that our optimization terms improve either accuracy or success rates. We performed an ablation study on the different losses to both the CAL and ALP models. First, we ablate the margin and modality loss for our CAL model in Table 2. Here, we see that with the addition of either margin or modality loss, we lose balanced accuracy, but increase success rate. However, by introducing both the margin loss and modality loss, we see the highest accuracy across settings, and the second highest success rate, validating the use of both terms together. In Table 3, we see that the ALP model improves in both balanced accuracy and success rate with the addition of each loss term individually. This shows that all of our loss terms contribute to increasing the accuracy of our model without trading off our ability to identify which samples we can classify using image data alone.

The confidence from our conformal intervals is well calibrated. Figure 6 shows that, for a wide range of values of α , the proportion of samples on which CAL incorrectly says we can abstain from genetic information falls substantially below the nominal rate. We see that the error rate scales roughly linearly with our α level, going only up to a 10% error rate with an $\alpha = .9$. We observe only a single outlier at $\alpha = 0.01$, where the error rate slightly exceeds the

nominal rate. These results show that our intervals achieve nominal coverage, even with marginal conformal intervals, with even high α values showing a relatively small error rate. This implies that no adjustment for simultaneous coverage of logits is necessary in practice; nonetheless, in the supplement, we show results using a more rigorous statistical determination of confidence for our conformal intervals.

4.2. Qualitative Results

Here, we analyze an example reasoning process from each of CAL and ALP. Figure 7 presents an example of the reasoning process of CAL with $\alpha=0.05$. Given an input image, CAL first compares the image to a set of image prototypes and applies conformal prediction to decide whether genetic information is necessary. When classifying the Xylosandrus crassiusculus in Figure 7 (Top), CAL identifies that genetic information could possibly sway its prediction, and measures the specimen's genetic sequence. When classifying the Argyria centrifugens in Figure 7 (Bottom), the margin between the predicted class logit and the next highest logit is sufficiently high that, with high probability, the genetic information would not change the models prediction from Argyria centrifugens.

Figure 4 provides an example reasoning process for ALP. Given an input image — in this case, a Megaselia steptoeae — ALP computes the similarity of the prototype at the root node to the image; if the similarity is high, it traverses right, otherwise it traverses left. This process repeats until either (1) in the case of the right path in Figure 4, a leaf node is hit, yielding a prediction without genetic information, or (2) in the case of the left path, a genetic prototype is hit, confirming that we must measure genetic information. In this case, ALP traverses the right path and correctly classifies the specimen as a Megaselia steptoeae using only image information.

5. Conclusion

In this work, we presented two multimodal extensions of ProtoPNet: Conformal Abstention Learning (CAL), and Abstention Learning ProtoTree (ALP). We showed that these methods match the strong performance of multimodal black box models while providing interpretability and often avoiding the need to measure expensive genetic data. Moreover, our conformal prediction framework introduced for Multimodal ProtoPNet is modular and can be applied to ensemble any unimodal models in such a way that expensive modalities can often be avoided.

The ability to avoid expensive data modalities has substantial positive impacts in practice. When monitoring rare or endangered species, it may allow researchers to avoid capturing or harming individuals of the target species, thereby preventing the resulting ecological harm. For med-

ical applications, doctors may be able to avoid running expensive or invasive tests.

While the conformal prediction approach used in CAL is effective, it is often overly conservative because we used a lightweight conformal prediction approach. Future work should consider more advanced conformal prediction methods. Additionally, this work considered two data modalities; in practice, there may be several modalities of interest, each with varying costs. Future studies should consider extending this abstention-based approach to larger numbers of modalities with varying associated costs.

References

- [1] Peter L Bartlett and Marten H Wegkamp. Classification with a Reject Option using a Hinge Loss. *Journal of Machine Learning Research*, 9(8), 2008. 2
- [2] Akosua Busia, George Dahl, Clara Fannjiang, David Alexander, Lizzie Dorfman, Ryan Poplin, Cory McLean, Pi-Chuan Chang, and Mark DePristo. A deep learning approach to pattern recognition for short DNA sequences. *bioArxiv*, 2018.
- [3] Chaofan Chen, Oscar Li, Daniel Tao, Alina Barnett, Cynthia Rudin, and Jonathan K Su. This Looks Like That: Deep Learning for Interpretable Image Recognition. Advances in neural information processing systems, 32, 2019. 2, 6, 7, 15, 16, 17
- [4] Chi-Keung Chow. An Optimum Character Recognition System using Decision Functions. *IRE Transactions on Electronic Computers*, 3(1):247–254, 1957. 2
- [5] Corinna Cortes, Giulia DeSalvo, and Mehryar Mohri. Learning with Rejection. In *International conference on algorithmic learning theory*, pages 67–82. Springer, 2016. 2
- [6] Victor Dheur, Matteo Fontana, Yorick Estievenart, Naomi Desobry, and Souhaib Ben Taieb. A Unified Comparative Study with Generalized Conformity Scores for Multi-Output Conformal Regression. arXiv preprint arXiv:2501.10533, 2025. 3, 11
- [7] Jon Donnelly, Alina Jade Barnett, and Chaofan Chen. Deformable ProtoPNet: An Interpretable Image Classifier Using Deformable Prototypes. In *Proceedings of the IEEE/CVF conference on computer vision and pattern recognition*, pages 10265–10275, 2022. 2, 7
- [8] Jon Donnelly, Zhicheng Guo, Alina Jade Barnett, Hayden McTavish, Chaofan Chen, and Cynthia Rudin. Rashomon Sets for Prototypical-Part Networks: Editing Interpretable Models in Real-Time. In Proceedings of the Computer Vision and Pattern Recognition Conference, pages 4528–4538, 2025. 2
- [9] Benjamin Flück, Laëtitia Mathon, Stéphanie Manel, Alice Valentini, Tony Dejean, Camille Albouy, David Mouillot, Wilfried Thuiller, Jérôme Murienne, Sébastien Brosse, et al. Applying Convolutional Neural Networks to Speed up Environmental DNA Annotation in a Highly Diverse Ecosystem. Scientific Reports, 12(1):10247, 2022. 2
- [10] Zahra Gharaee, ZeMing Gong, Nicholas Pellegrino, Iuliia Zarubiieva, Joakim Bruslund Haurum, Scott C. Lowe, Jaclyn

- T. A. McKeown, Chris C. Y. Ho, Joschka McLeod, Yi-Yun C Wei, Jireh Agda, Sujeevan Ratnasingham, Dirk Steinke, Angel X. Chang, Graham W. Taylor, and Paul Fieguth. A step towards worldwide biodiversity assessment: The bioscan-1m insect dataset, 2023. 6
- [11] ZeMing Gong, Austin Wang, Xiaoliang Huo, Joakim Bruslund Haurum, Scott C Lowe, Graham W Taylor, and Angel X Chang. CLIBD: Bridging Vision and Genomics for Biodiversity Monitoring at Scale. In *The Thirteenth International Conference on Learning Representations*, 2025. 1, 2, 7
- [12] Mikko Impiö and Jenni Raitoharju. Improving taxonomic image-based out-of-distribution detection with dna barcodes. In 2024 32nd European Signal Processing Conference (EU-SIPCO), pages 1272–1276. IEEE, 2024. 2
- [13] Jing Lei and Larry Wasserman. Distribution-free Prediction Bands for Non-parametric Regression. *Journal of the Royal Statistical Society Series B: Statistical Methodology*, 76(1): 71–96, 2014.
- [14] Oscar Li, Hao Liu, Chaofan Chen, and Cynthia Rudin. Deep Learning for Case-Based Reasoning Through Prototypes: A Neural Network that Explains its Predictions. In *Proceedings* of the AAAI conference on artificial intelligence, 2018. 2
- [15] Chiyu Ma, Brandon Zhao, Chaofan Chen, and Cynthia Rudin. This Looks Like Those: Illuminating Prototypical Concepts Using Multiple Visualizations. Advances in Neural Information Processing Systems, 36:39212–39235, 2023.
- [16] Chiyu Ma, Jon Donnelly, Wenjun Liu, Soroush Vosoughi, Cynthia Rudin, and Chaofan Chen. Interpretable Image Classification with Adaptive Prototype-Based Vision Transformers. Advances in Neural Information Processing Systems, 37:41447–41493, 2024. 2
- [17] Chloé Martineau, Donatello Conte, Romain Raveaux, Ingrid Arnault, Damien Munier, and Gilles Venturini. A survey on image-based insect classification. *Pattern Recognition*, 65: 273–284, 2017. 2
- [18] Loris Nanni, Matteo De Gobbi, Roger De Almeida Matos Junior, and Daniel Fusaro. Advancing Taxonomy with Machine Learning: A Hybrid Ensemble for Species and Genus Classification. *Algorithms*, 18(2):105, 2025.
- [19] Loris Nanni, Nicola Maritan, Daniel Fusaro, Sheryl Brahnam, Francesco Boscolo Meneguolo, and Maria Sgaravatto. Insect Identification by Combining Different Neural Networks. Expert Systems with Applications, 273:126935, 2025.
- [20] Meike Nauta, Ron Van Bree, and Christin Seifert. Neural Prototype Trees for Interpretable Fine-grained Image Recognition. In *Proceedings of the IEEE/CVF conference on com*puter vision and pattern recognition, pages 14933–14943, 2021. 2, 5, 6, 7
- [21] Harris Papadopoulos, Kostas Proedrou, Volodya Vovk, and Alex Gammerman. Inductive Confidence Machines for Regression. In *European conference on machine learning*, pages 345–356. Springer, 2002. 2
- [22] Alec Radford, Jong Wook Kim, Chris Hallacy, Aditya Ramesh, Gabriel Goh, Sandhini Agarwal, Girish Sastry, Amanda Askell, Pamela Mishkin, Jack Clark, Gretchen

- Krueger, and Ilya Sutskever. Learning transferable visual models from natural language supervision, 2021.
- [23] Dawid Rymarczyk, Łukasz Struski, Jacek Tabor, and Bartosz Zieliński. ProtoPShare: Prototypical Parts Sharing for Similarity Discovery in Interpretable Image Classification. In Proceedings of the 27th ACM SIGKDD Conference on Knowledge Discovery & Data Mining, pages 1420–1430, 2021. 2
- [24] Dawid Rymarczyk, Łukasz Struski, Michał Górszczak, Koryna Lewandowska, Jacek Tabor, and Bartosz Zieliński. Interpretable Image Classification with Differentiable Prototypes Assignment. In European Conference on Computer Vision, pages 351–368. Springer, 2022. 2
- [25] Chenguang Song, Ke Chao, Bingjing Jia, and Yiqing Shen. Multimodal Prototypical Network for Interpretable Sentiment Classification. *Scientific Reports*, 15(1):32939, 2025.
- [26] Samuel Stevens, Jiaman Wu, Matthew J Thompson, Elizabeth G Campolongo, Chan Hee Song, David Edward Carlyn, Li Dong, Wasila M Dahdul, Charles Stewart, Tanya Berger-Wolf, Wei-Lun Chao, and Yu Su. Bioclip: A vision foundation model for the tree of life, 2024. 7
- [27] Vladimir Vovk, Alexander Gammerman, and Glenn Shafer. Algorithmic Learning in a Random World. Springer, 2005. 2
- [28] Samuel Waggoner, Jon Donnelly, Rose Gurung, Laura Jackson, and Chaofan Chen. Creating Interpretable Deep Learning Models to Identify Species Using Environmental DNA Sequences. *Scientific Reports*, 15(1):27436, 2025.
- [29] Chong Wang, Yuyuan Liu, Yuanhong Chen, Fengbei Liu, Yu Tian, Davis McCarthy, Helen Frazer, and Gustavo Carneiro. Learning Support and Trivial Prototypes for Interpretable Image Classification. In Proceedings of the IEEE/CVF International Conference on Computer Vision, pages 2062–2072, 2023. 7
- [30] Chong Wang, Yuanhong Chen, Fengbei Liu, Yuyuan Liu, Davis James McCarthy, Helen Frazer, and Gustavo Carneiro. Mixture of Gaussian-Distributed Prototypes with Generative Modelling for Interpretable and Trustworthy Image Recognition. *IEEE Transactions on Pattern Analysis and Machine Intelligence*, 2025. 2
- [31] Guangchen Wang, Jinbao Li, Cheng Tian, Xitong Ma, and Song Liu. A Novel Multimodal Prototype Network for Interpretable Medical Image Classification. In 2023 IEEE International Conference on Systems, Man, and Cybernetics (SMC), pages 2577–2583. IEEE, 2023. 2
- [32] Jiaqi Wang, Huafeng Liu, Xinyue Wang, and Liping Jing. Interpretable Image Recognition by Constructing Transparent Embedding Space. In *Proceedings of the IEEE/CVF international conference on computer vision*, pages 895–904, 2021. 2, 6, 16
- [33] Frank Willard, Luke Moffett, Emmanuel Mokel, Jon Donnelly, Stark Guo, Julia Yang, Giyoung Kim, Alina Jade Barnett, and Cynthia Rudin. This looks better than that: Better interpretable models with protopnext, 2024. 3
- [34] Yuancheng Yang, Renkai Ying, and Chao Tong. ProtoMM: Interpretable Prototype-Based Multimodal Model for Brain Cancer Survival Prediction. *Journal of Imaging Informatics* in Medicine, pages 1–14, 2025. 2

Appendix

5.1. Additional Examples of Reasoning Processes

5.1.1. Conformal Abstention Learning

In Figure 7, we present two examples of the reasoning process of the Conformal Abstention Learning (CAL) ProtoP-Net. The first involves querying genetic information while the second does not. In Figure 8, we show another pair of examples, one of which involves genetic data.

In all four examples, the image network alone correctly classifies the sample. But, for two of the samples, CAL identifies that genetic information could change the prediction.

5.1.2. Abstention Learning ProtoTree

We present additional example reasoning processes for the Abstention Learning ProtoTree (ALP). In Figure 9, we show two correctly-classified samples that require querying only image data, and in Figure 10, we show two correctly-classified samples that require querying at least one instance of genetic data. During the hard traversal, each internal node—which has either an image prototype or genetic prototype—computes the maximum activation of its image/genetic prototype with the latent patches generated by the convolutional feature extractor. If the activation is greater than 0.5, the sample gets routed to the right child node, and left otherwise.

The majority of the activations in both images and genetic sequences are polarized, as in they are close to 0 or 1. This indicates that the model, in most cases, is confident about the presence (or lack thereof) of a prototype in an image. The concentrated portion of red on each heatmap reveals the location where a prototype activates highly on an input image.

6. Image Backbone Benchmarks

For the image ProtoPNets, we ran additional benchmarks on DenseNet and VGG-16. We report the results in Table 4.

Model	Blackbox	ProtoPNet
ResNet-50	78.32	79.06
Densenet-161	84.01	80.47
VGG-16	70.05	72.36

Table 4. Balanced accuracies (%) of blackbox and ProtoPNet modles using different backbone architectures.

We further trained CAL ProtoPNet models using these ProtoPNet models for initialization. The success rate and accuracy of these models are reported in Figure 5

Backbone	Balanced Accuracy	Success %	
ResNet-50	97.32	40.26	
Densenet-161	95.26	39.17	
VGG-16	95.22	26.62	

Table 5. CAL ProtoPNet balanced accuracies (%) and success rates (%) using different backbone architectures at $\alpha = .05$.

7. Multi Conformal Prediction

For full statistical rigor, we introduce a variation of CAL which uses M-CP to estimate a confidence region around the predicted genetic logit vectors [6]. To do this we apply CAL using the L_{∞} distance between the true and predicted genetic logits as a conformity score.

Although rigorous, this approach results in overly conservative confidence regions. In order to classify without genetic data, the model must be heavily regularized to favor image information. The accuracy suffers as a consequence, as shown in Figure 12.

Since the bounds are so conservative, increasing the confidence value α has no effect on accuracy up to $\alpha=0.95$. That is, up to $\alpha=0.95$, the model never mistakenly forgoes genetic information, as shown in Figure 11.

8. Experimental Setup

8.1. Genetic Backbone Architecture

The specifications of the genetic backbone are detailed in Table 6. We noticed that a deeper architecture was not necessary to achieve high balanced accuracy, so we opted for this relatively shallow network.

8.2. Dataset Processing

In the BIOSCAN-1M dataset, there are a total of 84,000 samples labeled at the species level. We use a train/validation/test split of 60/20/20, with a minimum of 10 samples per class, which leaves us with a dataset of 41,660 samples over 516 classes. Due to the heavy class imbalance of this dataset, we evaluate our models using balanced accuracy. During training, underrepresented classes are oversampled so that the model sees an equal distribution of samples from all classes.

We perform image augmentation during training by introducing random rotations, skews, shears, flips, and distortions. All images are normalized and cropped to the shape (3,224,224). The variable-length raw genetic data are sequentially one-hot encoded to C=4 channels (A, C, T, G) with unknown or missing base pairs encoded into $0\in\mathbb{R}^4$. We then augment each genetic sequence by introducing random genetic substitutions, insertions, and deletions—analogous to point and frameshift mutations in biology. Finally, the sequence is zero-padded to preserve consistent

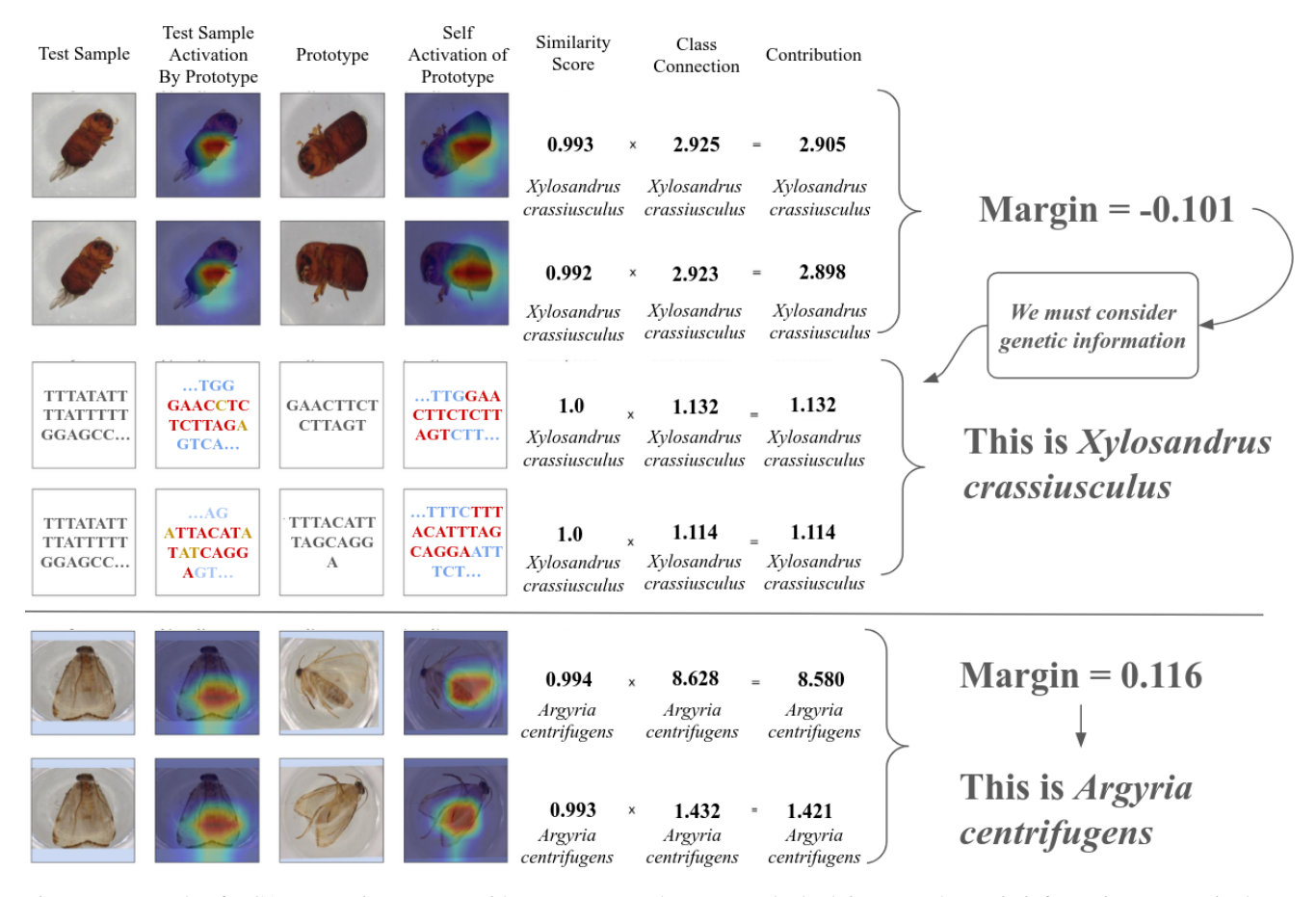


Figure 7. Example of a CAL reasoning process with $\alpha = .05$. For the top sample, both image and genetic information are required. For the bottom sample, only image information is required.

Layer	Type	Input Channels	Output Channels	Kernel Size	Stride	Padding
Conv1	Conv2D	4	16	(1,3)	(1,1)	(0,1)
	ReLU	16	16	_	_	_
Pool1	MaxPool2D	16	16	(1, 3)	(1, 3)	(0, 0)
Conv2	Conv2D	16	32	(1,3)	(1,1)	(0,1)
	ReLU	32	32	_	_	_
Pool2	MaxPool2D	32	32	(1, 3)	(1, 3)	(0, 0)
Conv3	Conv2D	32	64	(1,3)	(1,1)	(0,1)
Pool3	MaxPool2D	64	64	(1, 2)	(1, 2)	(0,0)

Table 6. Architecture of convolutional backbone for genetic data.

width, resulting in a shape of (4,1,720). Since the absolute position of nucleotides within a genetic sequence is meaningful, we add a sinusoidal positional encoding to the latent space.

8.3. Hyperparameters

8.3.1. Conformal Abstention Learning

When training a CAL ProtoPNet model, we initialize the constituent models for each modality with pretrained ProtoPNets. We initialize \hat{h} , the predictor linear layer, with the weights of the image linear layer $h^{(I)}$. We then train only the linear layers and modality weights.

We optimize hyperameters using a Bayesian optimiza-

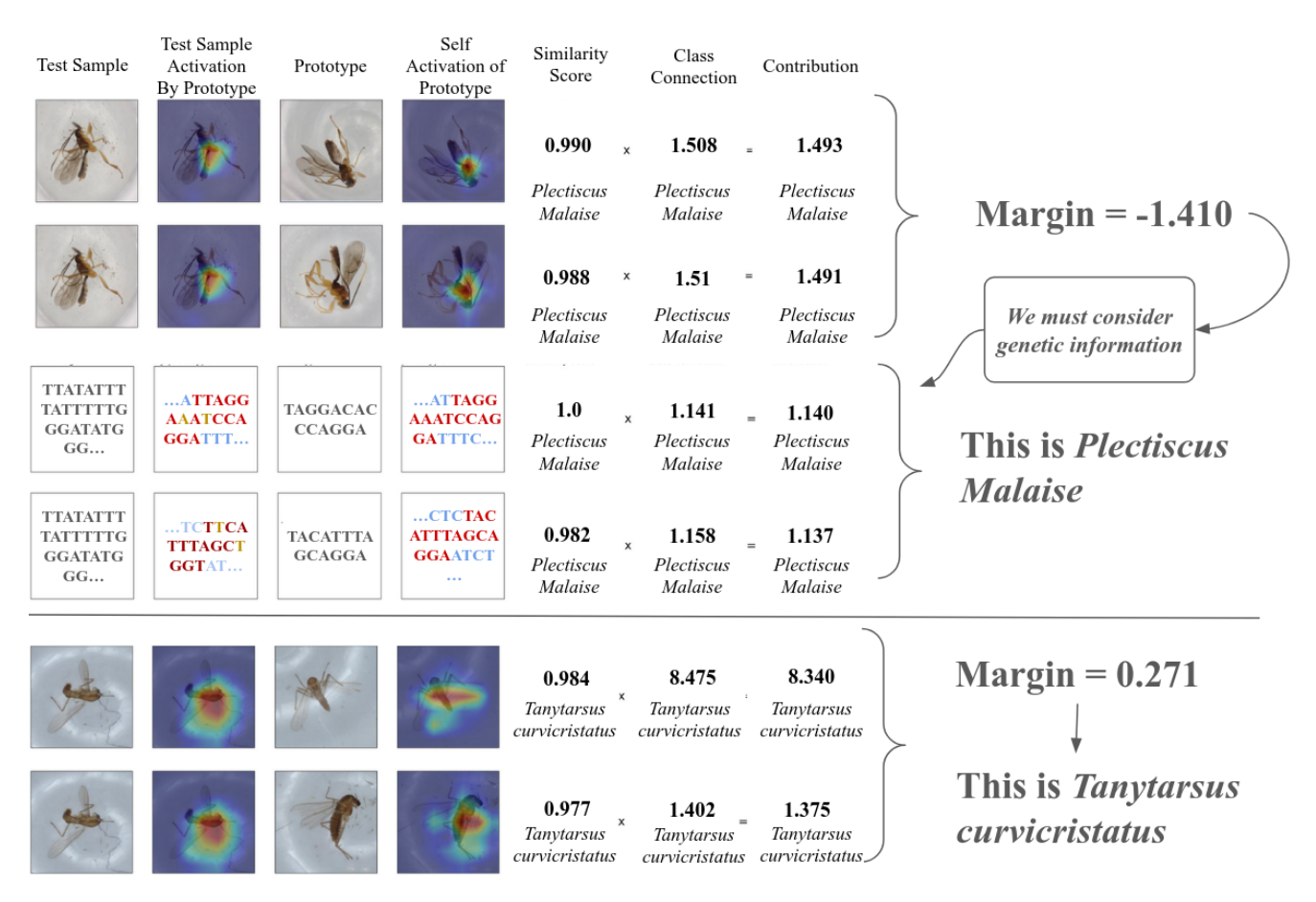


Figure 8. Another example of a CAL reasoning process with $\alpha=.05$. For the top sample, both image and genetic information are required. For the bottom sample, only image information is required.

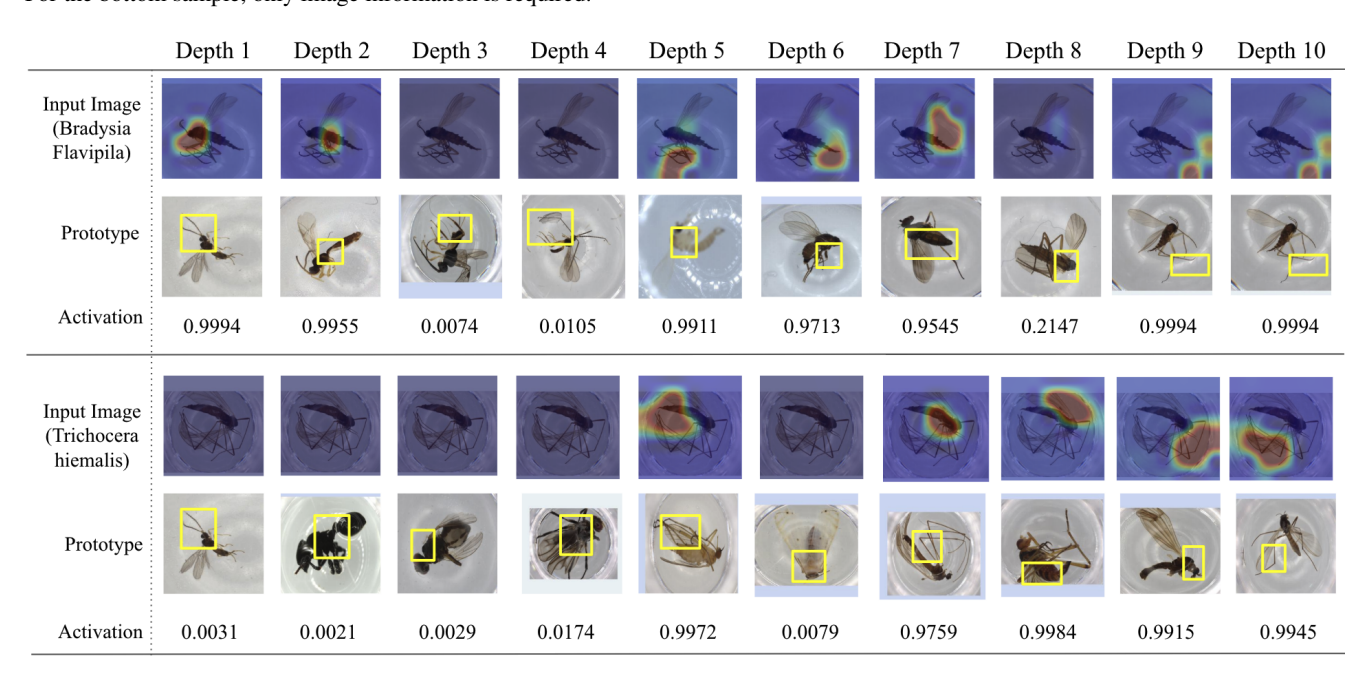


Figure 9. Reasoning path of ProtoTree for samples that require only image prototypes. Both input samples are correctly classified by the model.

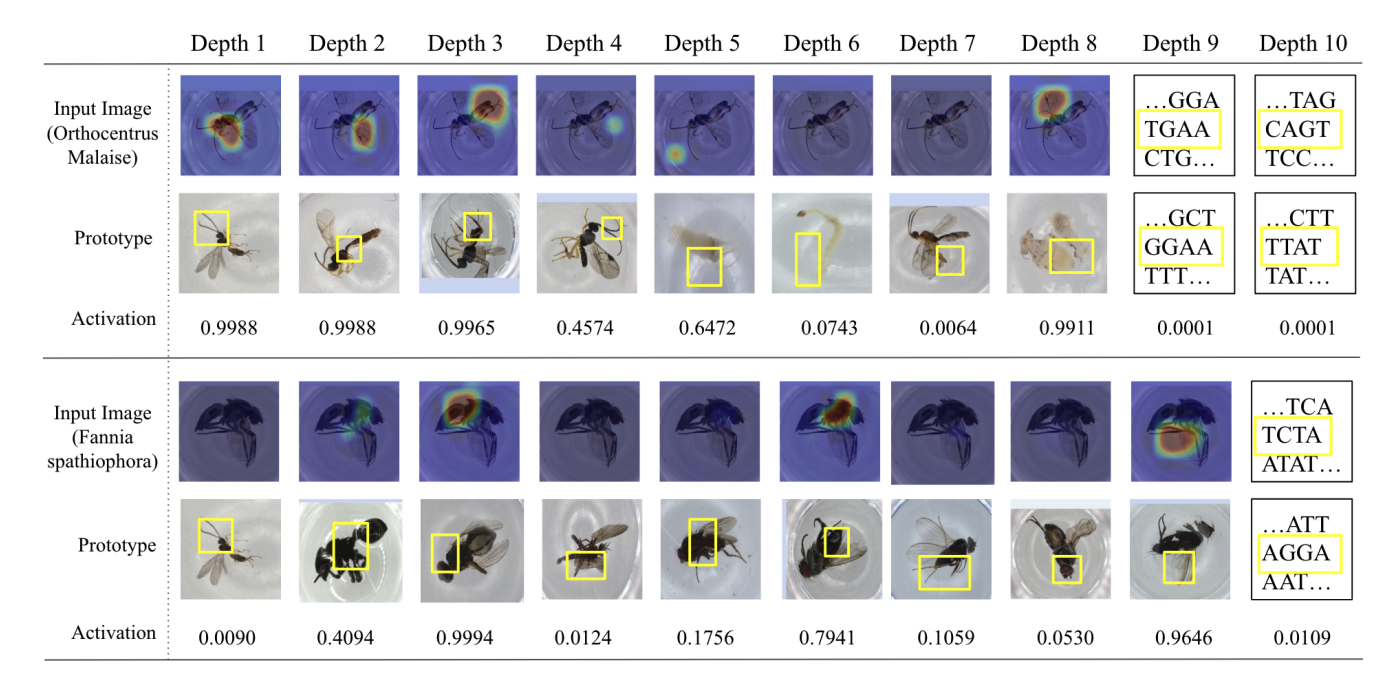


Figure 10. Reasoning path of ProtoTree for samples that require genetic prototypes. Both input samples are correctly classified by the model.

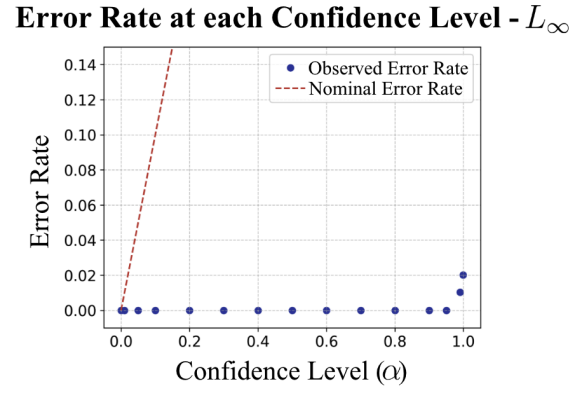


Figure 11. Error rate at each confidence level for the L_{∞} CAL model. Here, we see that M-CP CAL rarely incorrectly abstains from gathering genetic information.

tion scheme. The descriptions and prior distributions of all hyperparameter values can be found in Table 10.

We seek to maximize the following objective in our optimization on the validation set:

(Balanced Accuracy $_{\alpha=0.05}-0.9$) × Success Rate $_{\alpha=0.05}$

This objective was chosen to ensure that success rate and accuracy are simultaneously high and that the overall balanced accuracy of the model does not decrease far past that of the genetic ProtoPNet.

Success Rate and Accuracy at Different Confidence Values - L_{∞}

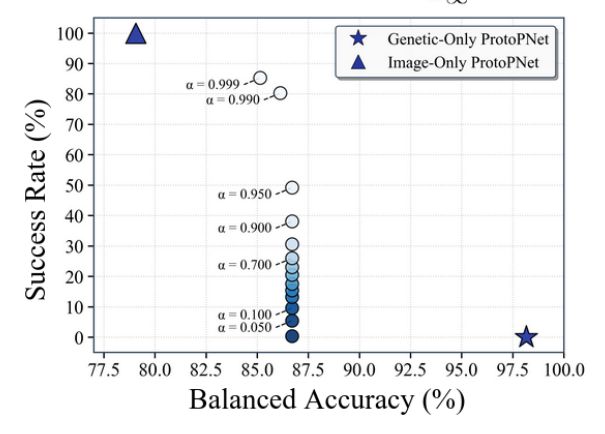


Figure 12. Success rate vs. balanced accuracy for our M-CP CAL model. The model performs approximately 12% worse than a plain genetic ProtoPNet model at most confidence values.

8.3.2. Abstention Learning ProtoTree

Due to the hard-traversal of the ProtoTree, the number of leaf nodes must be greater than the number of classes (516) in order for the model to have enough capacity to route each class to its own leaf node. Therefore, the image, genetic, and multimodal ProtoTrees were all trained with a depth of 10, which consists of 1023 prototypes and $2^{10} = 1024$ leaf nodes.

Hyperparameter Name	Distribution	ProtoPNet (Genetic)	ProtoPNet (Image)	Description
post_project_phases	Int Uniform	Min=2, Max=6	6	Number of post-projection phases
pre_project_phase_len	Int Uniform	Min=2, Max=6	Min=2, Max=7	Length of pre-projection phase
batch_size	Fixed	512	64	Number of samples per training batch
cluster_coef	Normal	$\mu = -0.8, \sigma = 0.5$	$\mu = -0.8, \sigma = 0.5$	Coefficient of the cluster loss from [3]
separation_coef	Normal	$\mu = 0.08, \sigma = 0.1$	$\mu = 0.08, \sigma = 0.1$	Coefficient of the separation loss from [3]
incorrect_class_connection	Fixed	0	-0.5	Inital weight between prototypes and differing class logits
joint_lr_step_size	Int Uniform	Min=5, Max=5	Min=2, Max=10	Step size for LR schedule
11_coef	Log Uniform	$Min=10^{-5}, Max=0.001$	$Min=10^{-5}, Max=0.001$	L1 regularization strength
activation_function	Fixed	cosine similarity	cosine similarity	Similarity function for prototype activation
base_latent_dimension	Fixed	2048	64	Depth of the latent space before la-
				tent_dim_multiplier_exp is applied
latent_dim_multiplier_exp	Int Uniform	Min=-3, $Max=3$	Min=-3, Max=3	Exponent controlling latent-dim scaling
lr_multiplier	Normal	$\mu = 1, \sigma = 0.4$	$\mu = 1, \sigma = 0.4$	Learning-rate scaling factor
num_addon_layers	Int Uniform	Min=0, Max=2	Min=0, Max=2	Number of additional layers before proto-
				type layer
num_prototypes_per_class	Fixed Values	5	10, 20	Number of prototypes allocated per class
phase_multipler	Fixed Values	1, 2	1, 2	Multiplier for training phase lengths
position_encoding_strength	Fixed Values	0.01, 0.05	_	Prototype feature position encoding strategy.
gen_aug_substitution_rate	Fixed Values	0, 0.025, 0.005, 0.01	_	Rate of nucleotide substitution for genetic augmentation
gen_aug_insertion_rate	Fixed Values	0, 2, 4	_	Number of inserted for genetic augmentation
gen_aug_deletion_rate	Fixed Values	0, 2, 4	_	Number of nucleotides deleted for genetic augmentation

Table 7. Hyperparameter search space for ProtoPNet.

Hyperparameter Name	Distribution	Values / Min-Max	Description
modality_reg_coeff	Uniform	Min=-2, Max=1	λ_1 , the regularization coefficient for modality weights
margin_loss_coeff	Uniform	Min=0, Max=0.5	λ_2 , the margin loss coefficient
predictor_mse_coeff	Log Uniform	$Min=10^{-3}, Max=1$	λ_3 , the coefficient for the mean squared error loss of
			the predictor
lr_multiplier	Log Uniform	Min=0.1, Max=1	Learning rate multiplier
modality_weight_optimization_epochs	Integer Uniform	Min=1, Max=6	Number of epochs to optimize the modality weights
			and last layers
ce_alpha	Fixed value	0.05	Conformal confidence level used for margin and cross
			entropy loss
batch_size	Fixed value	128	Number of samples per training batch
gen_aug_deletion_rate	Integer Uniform	Min=0, Max=4	Number of deletions applied during genetic data aug-
			mentation
gen_aug_insertion_rate	Integer Uniform	Min=0, Max=4	Number of insertions applied during genetic data aug-
			mentation
gen_aug_substitution_rate	Fixed values	0, 0.0001, 0.001, 0.005	Substitution rates applied during genetic data aug-
			mentation

Table 8. Hyperparameter search space for Multimodal ProtoPNet.

The embedding dimension for the image and genetic models were 2048 and 64 respectively. We used cosine similarity as the similarity metric in both cases.

In a unimodal ProtoTree, the backbone, add-on layers, and the prototype layer are optimized with separate learning rates, while the prediction head is optimized through a gradient-free update rule. Training a ProtoTree consists of two stages. In the initial "warm-up phase," we load and freeze the pretrained backbone and the prediction head, and we focus on training the add-on and prototype layers. In the "joint phase," all layers are trained. We optimize the hyperparameters using a Bayesian optimization scheme that maximizes the best validation balanced accuracy. The de-

scriptions and prior distributions of all hyperparameter values can be found in Table 9.

In our ALP, we initialize with the pretrained unimodal models and initialize both the modality weights and the logits in the leaves using threshold based modality assignment. We then optimize the hyperparameters in a similar fashion as done for the unimodal models, with descriptions and prior distributions of all hyperparameter values listed in Table 10.

8.4. Hardware and Software

Each experiment was conducted on a server consisting of 4 Intel Xeon E5-2640v4 CPU cores and a single RTX A5000 GPU with 24GB of memory. All models were run with Py-

Hyperparameter Name	Distribution	ProtoTree (Genetic)	ProtoTree (Image)	Description
warm_up_phase_len	Integer Uniform	Min=0, Max=50	Min=0, Max=25	The number of warm-up epochs before joint optimization begins
joint_phase_len	Integer Uniform	Min=0, Max=50	Min=0, Max=25	The number of joint optimization epochs
weight_decay	Log Uniform	$Min=10^{-4}, Max=1.0$	Min=0.1, Max=10.0	Regularization parameter for weight decay
num_addon_layers	Integer Uniform	Min=0, Max=3	Min=0, Max=2	The number of additional convolutional layers to add between the backbone and the prototype layer
batch_size	Fixed value	1024	128	Number of samples per training batch
gen_aug_substitution_rate	Uniform	Min=0.00, Max=0.01	_	Rate of nucleotide substitution for genetic data augmentation
gen_aug_insertion_rate	Integer Uniform	Min=0, Max=3	_	Rate of nucleotide insertion for genetic data augmentation
gen_aug_deletion_rate	Integer Uniform	Min=0, Max=3	_	Rate of nucleotide deletion for genetic data augmentation
cluster_coef	Uniform	Min=-1.5, Max=0.00	Min=-1.5, Max=0.00	Coefficient of the cluster loss from [3]
orthogonality_coef	Log Uniform	Min= 10^{-5} , Max= 10^{-1}	$Min=10^{-5}, Max=10^{-1}$	Coefficient of the orthogonality loss from [32]
backbone_lr	Log Uniform	$Min=10^{-5}, Max=10^{-2}$	$Min=10^{-4}, Max=10^{-2}$	Learning rate for the backbone network
add_on_lr	Log Uniform	$Min=10^{-4}, Max=10^{-1}$	$Min=10^{-4}, Max=10^{-2}$	Learning rate for the add-on layers
prototype_lr	Log Uniform	$Min=10^{-3}, Max=10^{-1}$	Min= 10^{-4} , Max= 3×10^{-2}	Learning rate for the prototype layer

Table 9. Hyperparameter search space for Image and Genetic ProtoTree.

Hyperparameter Name	Distribution	ProtoTree (Multimodal)	Description
warm_up_phase_len	Integer Uniform	Min=0, Max=50	The number of warm-up epochs before joint optimization begins
joint_phase_len	Integer Uniform	Min=0, Max=50	The number of joint optimization epochs
batch_size	Fixed value	128	Number of samples per training batch
gen_aug_substitution_rate	Uniform	Min=0.00, Max=0.01	Rate of nucleotide substitution for genetic data augmentation
gen_aug_insertion_rate	Integer Uniform	Min=0, Max=3	Rate of nucleotide insertion for genetic data augmentation
gen_aug_deletion_rate	Integer Uniform	Min=0, Max=3	Rate of nucleotide deletion for genetic data augmentation
cluster_coef	Uniform	Min=-1.5, Max=0.00	The value of λ_{clst} for clustering loss from [3]
orthogonality_coef	Log Uniform	$Min=10^{-5}, Max=0.1$	The value of λ_2 for orthogonality loss from [32]
variability_coef	Uniform	Min=-1.5, Max=0.00	The value of λ_3 for variability loss
weight_decay	Log Uniform	$Min=10^{-5}, Max=1.0$	The value of λ_4 for weight decay
routing_coef	Fixed	0.01	The value of λ_5 for routing loss
backbone_lr	Log Uniform	$Min=10^{-5}, Max=0.01$	Learning rate for the backbone network
prototype_lr	Log Uniform	Min=0.001, Max=0.1	Learning rate for the prototype layer
add_on_lr	Log Uniform	$Min=10^{-4}, Max=0.1$	Learning rate for the add-on layers

Table 10. Hyperparameter search space for Multimodal ProtoTree.

Torch v1.13.1 and CUDA version 11.3.

9. Local Analysis

In this section, we visualize the most similar prototypes to a given image/genetic input pair. We call this the *local analysis* of the input, as in [3]. We provide local analyses for a few samples from BIOSCAN-1M on both CAL and ALP.

9.1. Conformal Abstention Learning

Figure 13 shows the closest prototypes to two image samples and one genetic sample from a CAL ProtoPNet. Unsurprisingly, the most similar image prototypes come from the same species as the input. For sample 1, both of the

nearest prototypes correspond to the abdomen of the *Pletiscus Malaise*. For sample 2, both prototypes correspond to the upper legs of the *Pyropyga Incognita*. Both of the nearest prototypes to the genetic sample show a perfect match (activation of 1).

9.2. Abstention Learning ProtoTree

Figure 14 shows the local analyses of two image samples and one genetic sample from BIOSCAN-1M, where the prototypes are taken from a fully trained ALP with threshold t=0.8. In the figure, we observe semantic similarities between certain patches in the input image and the image prototypes such as the presence of spiny legs or a black hairy head in the species *Paradidyma Malaise*. For *Cram-*

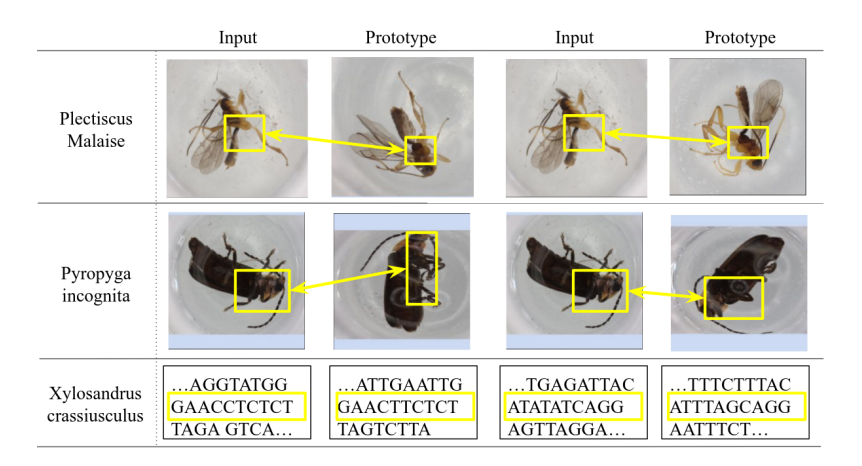


Figure 13. Local analyses of three test samples from BIOSCAN-1M for a CAL ProtoPNet. For each sample, we show the two most similar image or genetic prototypes in our model.

malaise Malaise, the model identifies prototypes indicating a brown ellipsoid body and large triangular wings. Again, the most similar image prototypes also come from samples that are of the same species as the input. The local analysis on the genetic input sequence shows a perfect match (activation of 1) with prototypes that have been projected to other samples of the same species.

10. Global Analysis

In this subsection, we visualize the most similar image and genetic samples to a given image or genetic prototype. We refer to this as *global analysis*, as in [3]. We provide global analyses for a few samples from BIOSCAN-1M on both CAL and ALP.

10.1. Conformal Abstention Learning

Figure 15 presents 4 prototypes—three image and one genetic—and shows the top 5 most similar samples to each of the prototypes learned by the CAL ProtoPNet. The prototypes visually match the corresponding patches of highest activation in the 5 samples. Furthermore, the closest genetic samples all match perfectly to the prototype with an activation of 1. Often, the most similar samples for a given prototype come from the same class as that of the prototype.

10.2. Abstention Learning ProtoTree

Figure 16 presents 4 prototypes—three image and one genetic. It shows the top 5 most similar samples to each of the prototypes learned by the ALP, which was trained with threshold t=0.8. Once again, each image prototype semantically matches the corresponding patches of highest activation in the top 5 samples, and each genetic prototype has a perfect match with corresponding genetic patches.

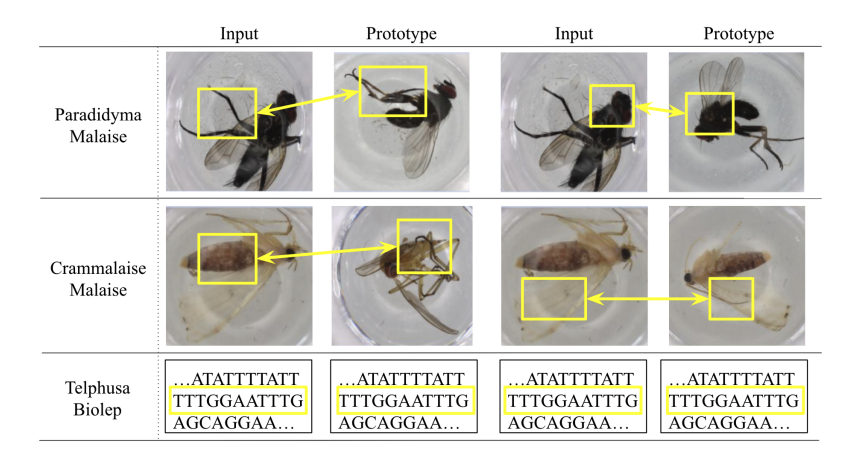


Figure 14. Local analyses of three test samples from BIOSCAN-1M for an abstention learning ProtoTree. For each sample, we show the two most similar image or genetic prototypes in our model.

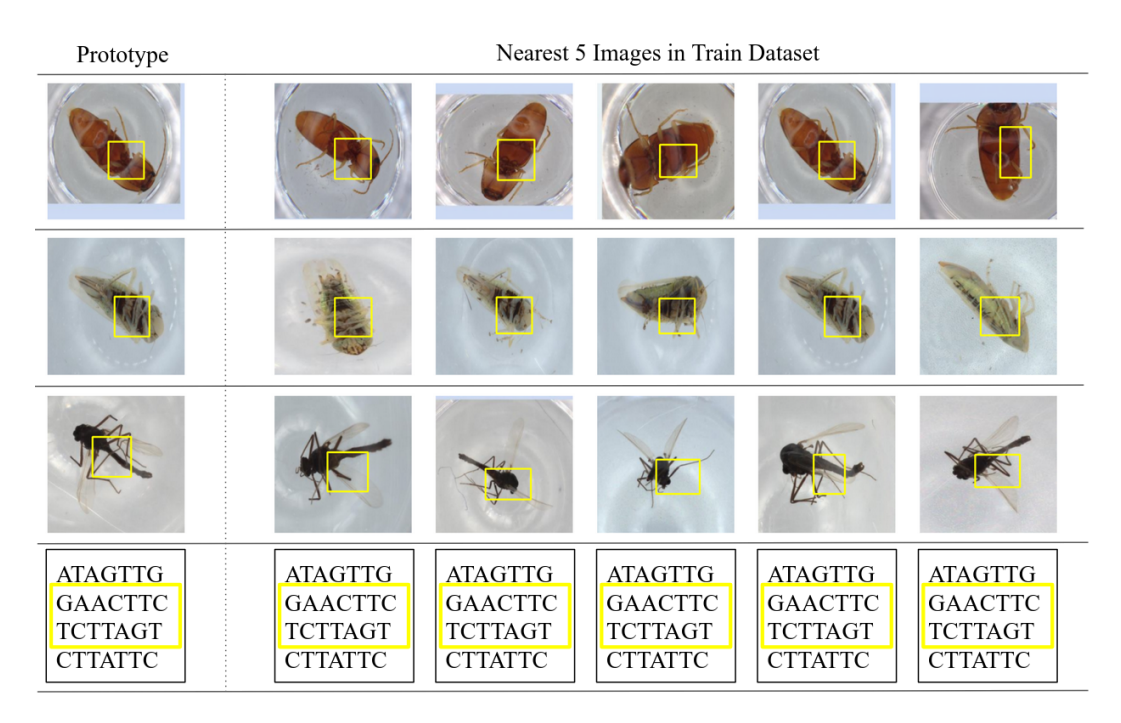


Figure 15. Global analyses of three image prototypes and one genetic prototype from BIOSCAN-1M for a CAL ProtoPNet. For each prototype, we show the 5 most similar images to the prototype.

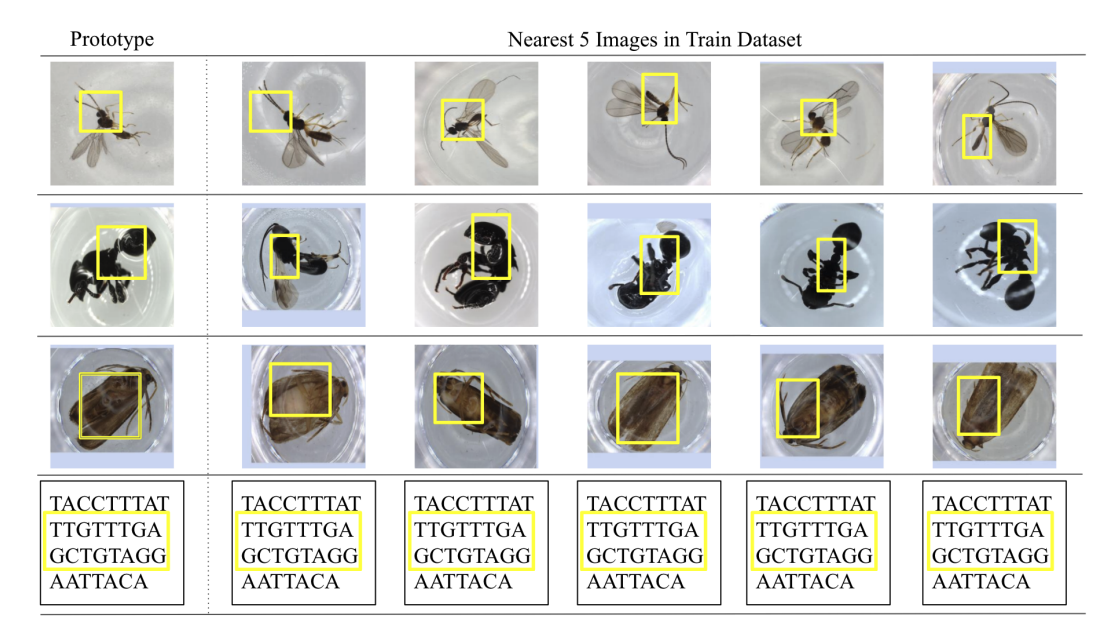


Figure 16. Global analyses of three image prototypes and one genetic prototype from BIOSCAN-1M for an abstention learning ProtoTree. For each prototype, we show the 5 most similar images to the prototype. We can describe the prototypes as such: a tiny head with long antennae (1st row), a black skinny thorax (2nd row), large brown rectangular wings (3rd row), and a genetic sequence (4th row).